Dinucleotide TpT and Its 2′-*O*-Me Analogue Possess Different Backbone Conformations and Flexibilities but Similar Stacked Geometries

Guillaume P. H. Santini,[†] Christophe Pakleza,[‡] Pascal Auffinger,[§] Céline Moriou,[||] Alain Favre,[⊥] Pascale Clivio,[#] and Jean A. H. Cognet*,[†]

Laboratoire de Biophysique Moléculaire, Cellulaire et Tissulaire, UMR 7033 CNRS, Université Pierre et Marie Curie, Genopole Campus 1, RN7, Evry 91030, France, Institute of Biochemistry and Biophysics, P.A.S., Pawinskiego 5a, 02-106 Warszawa, Poland, Architecture et réactivité de l'ARN, Université Louis Pasteur de Strasbourg, CNRS, IBMC, 15 rue René Descartes, 67084 Strasbourg, France, Institut de Chimie des Substances Naturelles, CNRS, 1 Avenue de la Terrasse, 91190 Gif sur Yvette, France, Institut Jacques Monod CNRS, Universités Paris 6 and 7, 75351 Paris, France, and FRE 2715, UFR Pharmacie, 51 rue Cognacq Jay, 51096 Reims cedex, France

Received: April 12, 2007

UV irradiation at 254 nm of 2′-*O*,5-dimethyluridylyl(3′-5′)-2′-*O*,5-dimethyluridine (**1a**) and of natural thymidylyl(3′-5′)thymidine (**1b**) generates the same photoproducts (CPD and (6−4)PP; responsible for cell death and skin cancer). The ratios of quantum yields of photoproducts obtained from **1a** (determined herein) to that from **1b** are in a proportion close to the approximately threefold increase of stacked dinucleotides for **1a** compared with those of **1b** (from previous circular dichroism results). **1a** and **1b** however are endowed with different predominant sugar conformations, C3′-*endo* (**1a)** and C2′-*endo* (**1b)**. The present investigation of the stacked conformation of these molecules, by unrestrained state-of-the-art molecular simulation in explicit solvent and salt, resolves this apparent paradox and suggests the following main conclusions. Stacked dinucleotides **1a** and **1b** adopt the main characteristic features of a single-stranded A and B form, respectively, where the relative positions of the backbone and the bases are very different. Unexpectedly, the geometry of the stacking of two thymine bases, within each dinucleotide, is very similar and is in excellent agreement with photochemical and circular dichroism results. Analyses of molecular dynamics trajectories with conformational adiabatic mapping show that **1a** and **1b** explore two different regions of conformational space and possess very different flexibilities. Therefore, even though their base stacking is very similar, these molecules possess different geometrical, mechanical, and dynamical properties that may account for the discrepancy observed between increased stacking and increased photoproduct formations. The computed average stacked conformations of **1a** and **1b** are well-defined and could serve as starting models to investigate photochemical reactions with quantum dynamics simulations.

1. Introduction

Skin cancer is the most common form of cancer in the United States and can be lethal if not treated properly.[1a] The conformation of DNA plays a central role in triggering specific photochemical reactions between adjacent pyrimidine nucleobases.[1b,c] However, the rules that govern the relationships between DNA conformational parameters and preferential photoproduct formation are still unclear. Elucidation of these rules is crucial to further understand photocarcinogenesis since photoproducts can exhibit different mutagenic properties.[2] One of the most remarkable results of UV induced DNA photochemistry is the quasi-exclusive formation[3a,b] of 5-(α-thyminyl)-5,6-dihydrothymine also called spore photoproduct (SP)[1] in A-DNA, whereas in B-DNA form and in living cells, dipyrimidine sites generate essentially two major types of photoproducts:[3c] the *cis-syn*-cyclobutane pyrimidine dimer (CPD) and the (6−4) pyrimidine pyrimidone photoproduct ((6−4)PP).[3] To elucidate the factors (conformation, solvent) involved in the photochemistry of the DNA double helix, it seems critical to acquire a deep understanding of those occurring at the dinucleotide level. This can be achieved by comparing the photochemistry of thymydilyl(3′-5′)thymidine (**1b**, TpT) with that of thymine−thymine dinucleoside monophosphate analogues endowed of particular conformational properties.[4,6] We compared the conformations and photochemical behavior of **1b** to the ones of 2′-*O*,5-dimethyluridylyl(3′-5′)-2′-*O*,5-dimethyluridine (**1a**: Figure 1), its bis 2′-α-methoxylated analogue.[6] NMR and circular dichroism studies clearly showed that while TpT does exhibit preferential C2′-*endo* sugar pucker, typical of the B-DNA form, its 2′-methoxylation increases the population of the C3′-*endo* sugar pucker, typical of A-DNA form. Typically, the fractions of sugar exhibiting C3′-*endo* pucker are 30 and 37% for TpT (**1b**) 5′ and 3′ ends, respectively, and rise to 75 and 66% for the corresponding position of methoxylated TpT (**1a**).[6] However, no spore photoproduct[6] could be detected in the photolysis of **1a** and **1b**, and the two dinucleotides were shown to generate exactly the same major photoproducts, that is, the CPD and the (6−4)PP.[6]

This leads to the paradox of similar photochemical reactions in two dinucleotides endowed of different conformations.[6] In

* Corresponding author. E-mail: cognet@ccr.jussieu.fr.
[†] Laboratoire de Biophysique Moléculaire, Cellulaire et Tissulaire.
[‡] Institute of Biochemistry and Biophysics.
[§] Université Louis Pasteur de Strasbourg.
[||] Institut de Chimie des Substances Naturelles.
[⊥] Institut Jacques-Monod.
[#] FRE 2715.

10.1021/jp0728656 CCC: $37.00
Published on Web 07/11/2007

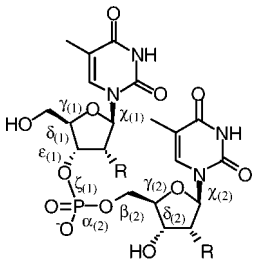

Figure 1. 2′-*O*,5-dimethyluridylyl(3′-5′)-2′-*O*,5-dimethyluridine (**1a**) and thymidylyl(3′-5′)thymidine (**1b**).

this paper, we first analyze quantitatively the photolysis kinetics of **1a** and **1b** to assess the quantum yields of CPD or (6−4) photoproducts formation. Then, we investigate this conformation−reaction paradox with a state-of-the-art molecular dynamics (MD) simulation and conformational adiabatic mapping.

According to the Franck−Condon principle, molecular excitation is fast (10^{-15} s) compared with nuclear motion. In dilute solutions, formation of cyclobutane dimers was shown to arise exclusively from the triplet state of thymine and uracil derivatives.[7] However, in stacked molecules or in the solid state, quantum efficiency was higher than the triplet quantum yield. This fact and other observations show that dimerization proceeds predominantly from the singlet states of the excited complex.[7] In TpT, the lifetime of singlet states of the excited thymine is on the order of 10^{-12} s.[7b] Therefore, photoproducts such as CPD or (6−4)PP are very likely to derive from the excitation of stacked molecules at the picosecond time scale.[7b] Both the nature of these photoproducts and their formation ratio can therefore be considered as probes into the detailed MD of the stacked complex. Conversely, because the first singlet states of the excited state are so short-lived, the detailed stacked conformations of dinucleotides in aqueous solvent with salt must be fully characterized to understand the photochemical behavior of **1a** and **1b**. One must therefore determine successively: (1) the extent of stacking between dinucleotides, (2) the extent of stacking within a dinucleotide in solution, with its lifetime, and (3) the three-dimensional (3-D) geometry of stacked dinucleotides, since unstacked conformations are not photoproductive.

(1) Early measurements of activity coefficients and studies by NMR showed that any mononucleoside, N, (where N stands for A, G, C, T, or U) prefers to stack in aqueous solution rather than to form base pairs.[8] Experimental studies of the dissociation of the stacked complex, $N \cdot N \leftrightarrows N + N$, give dissociation constants in the 1 to 2 M range at 25 °C in water for pyrimidine nucleosides.[9] As a result, concentration of the stacked complex is very low, in the micromolar range for millimolar solutions used within irradiation conditions of photochemical experiments.[8] This result extends likewise to dipyrimidine nucleotides and explains why photochemistry of dinucleotides does not lead to sizable amount of tetramers.

(2) Extensive studies of dinucleoside phosphates by absorption, circular dichroism (CD), optical rotary dispersion (ORD), NMR, and light emission showed that the two bases stack in solution.[8a,b] In many cases a simple two-state process, helical (stacked) $\leftrightarrows$ random coil (unstacked), is a good approximation to account for the major conformational changes of these dinucleotides.[8a,10,11a] Standard thermodynamic parameters, ΔH^0 and ΔS^0, indicate that melting temperatures at half-dissociation, Tm, are about room temperature or lower.[11a] The order of stacking for the dinucleoside phosphates (both ribo and deoxyribo) seems to be G ≈ A ≈ C > T or U.[8a] As a result, the concentration of the stacked complex for thymine dinucleotide is low, and to our knowledge, could not be measured accurately.[8c] 2′-Methoxylation of polynucleotides[12] or of dinucleoside phosphates[13] shifts the conformational equilibrium of the sugar pucker from the C2′-*endo* toward the C3′-*endo* conformation and increases the (stacking) thermostability of uniformly modified DNA. Measurements on closely related dinucleotide compounds indicate that relaxation times for the equilibrium between the stacked and the unstacked conformations in a dinucleotide are in the range of several nanoseconds.[8d]

(3) The 3-D conformation of stacked dinucleoside phosphates in aqueous solution is not accurately known but is analogous to that found in a single strand of double-stranded B-DNA or A-RNA with both bases anti in a right-handed helix as shown by numerous studies.[8a,13] Accordingly, the geometries of double-stranded DNA are used as the much-studied reference.[8,11,14] B-DNA and A-RNA can be generated with two different sets of parameters, R roll (rotation) and S slide (translation) and T twist (rotation),[14c,d] showing that their stacking geometries are different both at the levels of the helices and at those of the base pairs.[14a] Stacking is a dominant force that stabilizes the helix structure.[15] An important point for this study is that stacking of single unpaired bases at the end of a duplex is observed to have a different stabilizing effect in B-DNA or A-RNA. For B-DNA, the stacking of the unpaired base is more favorable on the 5′-end than on 3′, whereas for A-RNA it is the opposite.[15] Presumably, this is due to the different geometries of base stacking in A-RNA and B-DNA. Taken together, all of these observations could suggest that stacking geometries of **1a** and **1b** are different.

Early computer simulations began to explore the conformational characteristics of dinucleoside monophosphates including d(TpT) by molecular mechanics.[16] In agreement with experiments, computation of free energies of stacking demonstrates the importance of solvent and of its explicit treatment.[17] As shown in detail by different reviews,[18] computer simulations now make it possible to explore dynamic conformations of nucleic acids to a fine degree mostly through nanosecond length dynamics simulations in explicit solvent thanks to fast particle mesh Ewald (PME) methods. These methods are now capable of resolving apparent contradictions embedded in experimental observations designed to question the physics of stacking.[19] MD simulations have also recently explored the differential flexibility of DNA and RNA double-stranded molecules.[20] Using these implementations, new MD simulation protocols have been developed and reviewed.[21] They showed "that a remarkable level of atomic and dynamic resolution can be obtained".[18a] Here, we use these MD protocols to investigate the dynamic conformation of 2′-*O*,5-dimethyluridylyl(3′-5′)-2′-*O*,5-dimethyluridine **1a** and thymidylyl(3′-5′)thymidine **1b** by unrestrained molecular simulation in explicit solvent and salt. Our main purpose is to understand how the different conformations of the stacked compounds, with **1a** mostly in A-form conformation and **1b** mostly in B-DNA, can lead unexpectedly to the same type of photochemistry, with different yields.

2. Experimental and Computational Procedures

2.1. Photolysis Kinetics. The following scheme summarizes the equilibrium in solution between Du, the random coil unstacked dinucleotide conformation, and Ds its helical stacked

conformation, and the photochemical reaction where Ds* is the excited state, and P is a photoproduct, CPD or (6−4):

$$\mathrm{Du} \underset{10^{-9}\ \mathrm{s}}{\longleftrightarrow} \mathrm{Ds} \underset{k_d\,(10^{-12}\ \mathrm{s})}{\overset{h\nu\,(10^{-15}\ \mathrm{s})}{\rightleftharpoons}} \mathrm{Ds}^* \xrightarrow{k_p} \mathrm{P}$$

For a monomolecular equilibrium in absence of irradiation, the ratio Ds/(Du + Ds) is independent of the concentration of D = Du + Ds. Under stationary monophotonic irradiation conditions, this ratio remains unaffected since (a) the fraction of molecules in the excited state (Du* or Ds*) is negligible as compared with Du + Ds and (b) the overall rate of the reaction is extremely slow (in the minutes range) compared with the time scale of the Du ⇆ Ds equilibrium (nanosecond range).

Therefore, it is as if the photochemical reaction was a very fast probe (picosecond range) of different stacked conformations in an unperturbed equilibrium with unstacked states (nanosecond range). The rate equation is:

$$\frac{dP}{dt}\,(\text{mole min}^{-1}) = Ia\,(\text{Einstein min}^{-1})\,\frac{k_p}{k_p + k_d}$$

Here, *Ia* is the light absorbed by Du + Ds, k_p is the reaction rate, and $k_d \approx 6 \times 10^{13}\ \text{min}^{-1}$, the deactivation rate. We ignore which fraction of D is on the stacked form Ds. Therefore, we determine apparent quantum yields related to the true quantum yield, $\Phi = k_p/(k_p + k_d)$ by: $\Phi_{\text{measured}} = \Phi(\text{Ds}/(\text{Du} + \text{Ds}))$. Irradiation conditions are chosen so that sizable molar fractions of the photoproducts are formed over ~30 min (Figure 2). Under these conditions, initial rates can be measured with $t < 10$ min.

An aqueous solution (1500 μL, HPLC grade) of a 1/1 mixture of compound **1a** and **1b**, ($OD_{max} = 6.3$ for each solution) was prepared in a quartz cuvette (0.5 cm optical path). The oxygen of the solution was removed by argon bubbling during 30 min, and then, the solution was exposed for 30 min to the 253.7 nm light source (2 × 15 W, VL 215C Lamp, Vilber Lourmat, Marne la Vallée, France). This low-pressure and low-power mercury lamp was designed to be practically monochromatic at 253.7 nm. It does not produce any sizable irradiation band at 210 nm that would cause the photochemical reversion of CPD. Irradiation bands above 253.7 nm, and in particular at 320 nm that could cause the formation of the Dewar photoadduct from (6−4), have very low intensities and are within the spectrum signal-to-noise ratio. This type of lamp is a convenient substitute for the high-pressure and high power (1000 W) mercury arc lamp equipped with a monochromator used in reference experiments.[22a] The entire photochemical behavior of TpT in our control kinetics experiments is identical (to within 1 or 2%) to those of Johns et al. [22a] with the monochromator apparatus. Note also here, kinetics analyses are limited to the determination of initial rates where the irradiation of photoproducts is negligible. An aliquot of the solution was sampled at $t = 0$, 2, 4, 6, 8, 10, 15, 20, and 30 min and analyzed by reverse-phase HPLC.

Twenty-five microliters of the irradiation mixture was injected on a SYMMETRY C18 (5 μm, 4.6 × 250 mm) column using a 50 min, 1 mL/min gradient of 0−15% in 0.05 M aqueous ammonium acetate. Elution peaks corresponding to **1a**, **1b**, and their major photoproducts were followed by their 230 nm absorbance using a photodiode detector.[6] The surface peaks were measured and converted into the corresponding molar amounts of product assuming that **1a** and **1b** have the same molar extinction coefficients at 230 nm. Absorption spectra of **1a** and **1b** between 200 and 400 nm are practically superimposable, and the difference in molar extinction coefficients is due to the difference (estimated < 3%) between two small hypochromic effects.[22b−d] The same approximation was applied for CPDs on the one hand and (6−4)PPs on the other.

Accordingly, the molar fraction of **1a** (or **1b**) converted into any of its photoproducts, P, was obtained by multiplying the ratio $\Delta S_p/\Delta S_0$ (ΔS_p and ΔS_0 are respectively the peaks areas corresponding to P at time *t* and to **1a** (**1b**) at time 0) by 1.325 for CPDs and by 0.726 for (6−4)PPs. The ϵ_{230} values were taken from Johns et al. (see p 514: ϵ_{230} **1b** = 5300 L M^{-1} cm^{-1}; ϵ_{230} CPD TpT = 4000 L M^{-1} cm^{-1}; and ϵ_{230} (6−4)PP TpT = 7300 L M^{-1} cm^{-1}).[22a]

Quantum yields for the formation of **1a** photoproducts were evaluated by comparing their initial rates of formation with those of the corresponding photoproducts of **1b**, assuming for the latter the values established before. [22a]

2.2. MD Simulations. MD simulations were performed using the AMBER 5 and 7 packages and the PARM98 force field.[23] The partial charges of the modified ribose moieties of **1a** were taken from Venkateswarlu et al.[24] The initial conformations of each dinucleotide, **1a** and **1b**, were generated as a single-stranded stacked standard, A and B form, respectively.[25] The dinucleotides were placed in a box that contained 1054 (**1a**) or 1030 (**1b**) TIP3P water molecules, $6K^+$, and $5Cl^-$ ions corresponding to a concentration close to 0.25 M of added KCl. Target temperature and pressure were set at 298 K and 1 atm, respectively. The simulation protocols were identical to those described by Auffinger et al.[20b,c] The equilibrium phase lasted 400 ps after which 10 ns MD trajectories were generated. An integration step of 0.002 ps was used. The **1a** and **1b** molecules remained stacked during most of the MD runs. Molecular structures were recorded every 0.1 ps for analysis.[26] These two MD runs are presented in detail in the result section. Several control MD runs were performed. The influence of the starting geometry on the stacking geometry could be ruled out by MD runs where the initial conformation of **1a** was B-DNA or that of **1b** was A-DNA.

2.3. Average MD Structures. They represent a convenient and practical means to compare MD runs if the conformation populations are well-distributed about a single conformation. They are defined and constructed with a two-step procedure: (1) computation of averages of the backbone and glycosidic torsion angles, $\theta_{i,0}$, from 10 ns MD simulations and (2) construction of the average molecular conformation by energy refinement with AMBER under constraints of torsion angles, $\theta_{i,0}$. Torsion angles, θ_i, were forced to set values, $\theta_{i,0}$, by addition of $E = \sum_i k(\theta_i - \theta_{i,0})^2$ to the energy function of AMBER. The constant *k* was set equal to 900 kcal/(mol·rad^2).

2.4. Fitting Procedures. Calculations of the axis, the cylinder, and the trajectory of the helix (Figures 4 and 5) were obtained by superimposing the average molecular dinucleotide conformations onto a standard A- or B-form helix.[25] Superimposition of molecular conformations is achieved by rigid body translations and rotations.[27]

The mean plane of a sugar (Figure 5) is defined here by a point and a normal vector. The point is the geometric center of the five atoms of the sugar ring. The normal vector is the average of all possible normal vectors to the planes that pass through any three distinct atoms taken out of the five of the sugar ring.

2.5. Adiabatic Maps. Adiabatic maps of the total potential energy were computed by energy refinement of **1a** or **1b** with a series of small deformations along two deformation coordinates. As stated by McCammon and Harvey,[28] it can be thought of as an approximation to the enthalpic component of the potential of mean force. Torsion angles, δ_i, of the two nucle-

otides, *i*, are the deformation variables and were varied as explained elsewere.[29] Torsion angles were forced to set values by addition of $E = \sum_i k(\delta_i - \delta_{i,0})^2$ to the energy function of AMBER as explained in section 2.3. In the first stage, each starting structure was first identified as close to the global minimum where the norm of the gradient was less than 0.05 kcal/Å under torsion angle constraints. These structures were relaxed without constraints until the norm of the gradient was less than 0.0001 kcal/Å and were subsequently used to build the final map. In the final stage, refinement under constraints of all conformations until the norm of the gradient was less than 0.0001 kcal/Å was sufficient to obtain contour maps at a resolution of 2° torsion angle from 50 to 170° in both dimensions (Figure 5).

3. Results and Discussion

3.1. Comparative Photolysis Kinetics by HPLC. We have previously reported the comparative qualitative photolysis and HPLC analysis of **1a** and **1b**.[6] Herein, to determine the quantum yield of photoproducts formation in the **1a** series, we analyzed the photolysis kinetics of **1a** with respect to the one of **1b** at short time of irradiation.

To compare directly the photochemical behavior of **1a** and **1b**, these compounds were irradiated at 254 nm as an aqueous equimolar mixture. Samples were analyzed by HPLC at 0, 2, 4, 6, 8, 10, 15, 20, and 30 min. Figure 2 shows the molar fraction

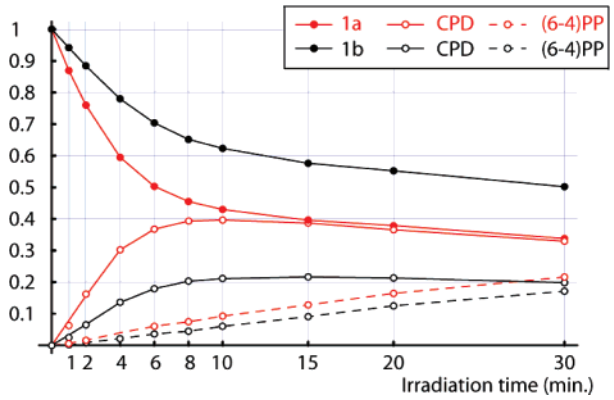

Figure 2. Molar fractions of **1a**, **1b**, and of their respective photoproducts as a function of irradiation time.

of **1a**, **1b**, and of their respective photoproducts as a function of irradiation time. Up to 4 min, all kinetics are linear. Then, they deviate from linearity. This is essentially due to the reversibility of the CPD formation process.

Figure 2 shows clearly that **1a** is more photoreactive than **1b**. At initial times of the photoreaction ($t < 10$ min), the former disappears faster, and accordingly, the initial rates of formation of the photoproducts of **1a** are higher than those corresponding to **1b**.

The quantum yields (at 254 nm) of photoproducts formation in the **1a** series were determined with respect to those reported by Johns et al.[22a] for the **1b** series. Table 1 shows that, taking into account experimental errors, the ratios of the quantum yields for formation of CPD over (6−4)PP, 14.0 for **1a** versus 11.0 for **1b**, are not very different. Equivalently, the ratio of quantum yields of formation of CPD for molecules **1a** and **1b** (2.7) is not very different from that of (6−4)PP (2.15). Therefore, no large bias for the formation of one class of photoproduct is observed in the case of **1a** compared to that of **1b**.

3.2. Average Percentages of C3′-*endo* Conformations Observed by MD and by NMR. Analyses of the 10 ns MD

TABLE 1: Quantum Yields of CPD and (6−4) Photoadduct Formation for Molecules 1a[a] and 1b[b]

	quantum yields Φ	
	CPD	(6−4)PP
1a	$(3.0 \pm 0.17) \times 10^{-2}$	$(2.15 \pm 0.1) \times 10^{-3}$
1b	$(1.1 \pm 0.05) \times 10^{-2}$	$(1 \pm 0.05) \times 10^{-3}$
ratio **1a**/**1b**	2.7 ± 0.27	2.15 ± 0.2

[a] Calculated from the linear part of the dose-curve of the corresponding photoproduct; standard deviations are estimated from five measurements. [b] Johns et al.;[22a] standard deviations are estimated from p 513.

trajectories with explicit water molecules showed that the two thymines within **1a** and **1b** remained stacked over most of the simulations when their starting conformation was A and B, respectively. A relatively stable behavior of the stacked conformation was observed previously for r(GpU) over 2 ns with the CHARMM program.[17c] For **1b**, our MD simulations showed that the trajectories were independent of the initial A or B conformation (see section 2.2). This observation suggests that equilibrium conformations of the stacked structures could be reached rapidly with these small molecules. In the case of **1a**, when the MD simulation was performed with an initial B conformation, the two thymines tended to unstack, a phenomenon likely due to the C2′-*endo* sugar pucker of the 5′ residue that gives rise to unfavorable steric interactions with the adjacent 3′-sugar as observed before.[30] Unstacked conformations of dinucleotides are not photoproductive and therefore were not explored further.

The percentages of C3′-*endo* conformations in 10 ns MD runs performed for the stacked molecules, **1a** and **1b,** with initial A-DNA and B-DNA conformations, respectively, are reported in Table 2. Detailed average glycosidic and backbone torsion angles, pucker amplitude $\Phi_{(i)}$, and pseudorotation phase angle

TABLE 2: Average Percentages of C3′-*endo* Conformation Computed over 10 ns MD Runs for the 5′ and 3′ Residues of Stacked Molecules 1a and 1b[a]

	10 ns MD simulations	
	(residue 1) 5′ end	(residue 2) 3′ end
1a	100% (75%)	77% (66%)
1b	5% (30%)	24% (37%)

[a] Numbers in parenthesis are experimental data from previous NMR studies for the mixture of stacked and unstacked molecules in equilibrium.[6] C3′-*endo* conformations are defined to be consistent with the boundary line observed in adiabatic maps of Figure 6: C3′-*endo* when $\delta < 113°$ and C2′-*endo* when $\delta > 113°$. This approach is consistent with the usual interpretation of NMR data.[13a]

$P_{(i)}$ of the sugar residues computed from 10 ns MD are reported in Table 3. The major conformation of sugar puckers was C3′-*endo* for **1a** and C2′-*endo* for **1b**. In both cases, these major conformations were more predominant for the 5′ residue than for the 3′ residue. These two results pertain only to stacked molecules and cannot be compared directly to NMR observations because the populations of pucker conformation in stacked or unstacked molecules are difficult to assess experimentally.[13] Nevertheless, they are in good qualitative agreement with experimental findings on sugar puckers for the following reasons. In a stacked dinucleoside monophosphate, the number of degrees of freedom is reduced. This is clearly the case for the stacked conformations **1a** and **1b** that are well-defined as shown by the small values of most standard deviations in Table 3. In unstacked states, many more degrees of freedom exist, and a large number of distinct conformers exist in

TABLE 3: Average Glycosidic and Backbone Torsion Angles $\alpha_{(i)}$, $\beta_{(i)}$, $\gamma_{(i)}$, $\delta_{(i)}$, $\epsilon_{(i)}$, $\zeta_{(i)}$, $\chi_{(i)}$ (see Figure 1a), Pucker Amplitude $\Phi_{(i)}$, and Pseudorotation Phase Angle $P_{(i)}$ (in Degrees) of the Sugar of Residue i[a] Computed from 10 ns of MD Simulations Performed with Initial A-DNA (1a) and B-DNA (1b) Conformations[b,13]

	$\gamma_{(1)}$	$\delta_{(1)}$	$\epsilon_{(1)}$	$\zeta_{(1)}$	$\chi_{(1)}$	$\alpha_{(2)}$	$\beta_{(2)}$	$\gamma_{(2)}$	$\delta_{(2)}$	$\chi_{(2)}$	$\Phi_{(1)}$	$P_{(1)}$	$\Phi_{(2)}$	$P_{(2)}$
1a	55	77	−146	−59	−163	−73	175	59	79	−149	42	10	39	14
	(12)	(7)	(15)	(12)	(10)	(11)	(10)	(8)	(7)	(13)	(5)	(11)	(6)	(11)
1b	149	138	−170	−83	−118	−69	171	53	123	−109	43	153	41	128
	(62)	(15)	(15)	(11)	(19)	(11)	(10)	(10)	(19)	(22)	(6)	(29)	(6)	(36)

[a] $i = 1$ corresponds to the 5′ residue and $i = 2$ to the 3′ residue. [b] For **1a**, the average conformation was computed over 7.7 ns when both sugars are in C3′-*endo*-C3′-*endo*, whereas for **1b** it was computed over the entire MD run dominated by the C2′-*endo*-C2′-*endo* conformation. Numbers in parentheses correspond to standard deviations from average values.

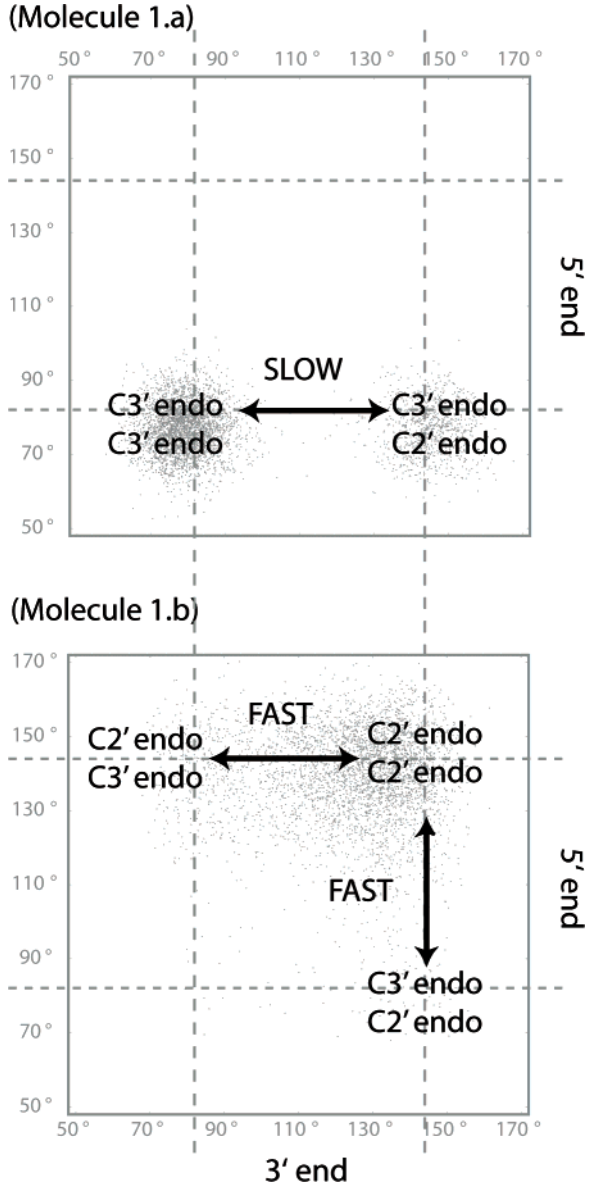

Figure 3. Schematic view of the major conformational changes observed in 10 ns MD runs for molecules **1a** and **1b**. For **1a**, conformational changes are rare and occur on a nanosecond time scale, whereas for **1b**, they are frequent at the scale of a few picoseconds. Note that, in both cases, transition between conformations takes place in about one picosecond.[28]

solution.[13,31] In the case of **1a**, stabilization of the C3′-*endo* conformation by 2′-*O*-methylation is primarily due to the steric interaction among the pyrimidine base, the 2′-*O*-methyl group, and the 3′-phosphate group.[13d] This steric interaction explains in particular why the C3′-*endo* conformation is more populated on the 5′ than on the 3′ residue as observed both experimentally and in our MD runs (cf. Table 2). Because unstacked conformers are less constrained, their populations of C3′-*endo* conformation should be less important than in the stacked conformers. The experimental value observed by NMR[6] is an average over stacked and unstacked dinucleotide conformations. Therefore, and in agreement with our findings, it should probably be taken as a lower estimation for the percentage of C3′-*endo* in the stacked conformation. In the case of **1b** and more generally for all possible deoxy-dinucleotides, NMR data indicate that the C3′-*endo* conformation ranges from 19 to 33% for the 5′ residue and from 31 to 41% for the 3′-nucleotidyl unit.[13b] It is higher for the 3′ residue than for the 5′ residue as observed in our MD runs. In purine dinucleotides, the percentage of stacked molecules is probably high enough for these observations to be indicative of the stacked conformation. However, in TpT, this percentage is too small and NMR observations are mostly indicative of the conformation of unstacked molecules. Therefore, NMR observations of TpT dinucleotides pertain mostly to unstacked conformations, while our MD results pertain to stacked conformations.

At a more detailed level, in the case of dinucleotide **1a**, MD pucker conformations as a function of time suggest that the major stacked conformation, all C3′-*endo*, is in slow equilibrium on the nanosecond time scale with the minor stacked conformation, C3′-*endo*-C2′-*endo*. In the case of dinucleotide **1b**, there is a rapid equilibrium on the picosecond time scale between different conformations: a major conformation in which both sugars are in the C2′-*endo* puckering mode, minor conformations with one of the two sugars in the C3′-*endo* form as shown by the average and large standard deviation values of $P_{(1)}$ and $P_{(2)}$ (153 and 128°, respectively, rmsd ≥30°) and of $\delta_{(1)}$ and $\delta_{(2)}$ (138 and 123°, respectively, rmsd ∼ 17°; Table 3), and also by their detailed trajectories as a function of time. These two different families of dynamical equilibria are summarized in Figure 3 (see also Figure 6).

3.3. Average Stacking Geometry of 1a and 1b is Similar in 10 ns MD Runs. Even though these small molecules tumble in solution during MD runs as observed before,[17c] the average structures of the major, all C3′-*endo*, stacked conformation for **1a** over 7.7 ns and the average structure of **1b** over 10 ns are well-defined and could be constructed from the average pucker phases and torsion angles of Table 3. These average conformations are compared by means of two different modes of superimpositions to reveal their specific conformational elements (Figure 4). On the one hand, as illustrated in Figure 4a, superimposition of the averaged molecular structure of **1a** (red) and **1b** (black) showed that they possess a very close backbone conformation (close average values of backbone torsion angles $\epsilon_{(1)}$, $\zeta_{(1)}$, $\alpha_{(2)}$, $\beta_{(2)}$, and $\gamma_{(2)}$) but very different sugar puckers (P and δ) and glycosidic torsion angles (χ). On the other hand, superimposition of the two structures by adjustment of the 3′-base atoms alone (Figure 4b) demonstrates that the 5′-thymines of **1a** and **1b** share nearly the same relative positions in space. These two bases are (i) contained in the same plane, (ii)

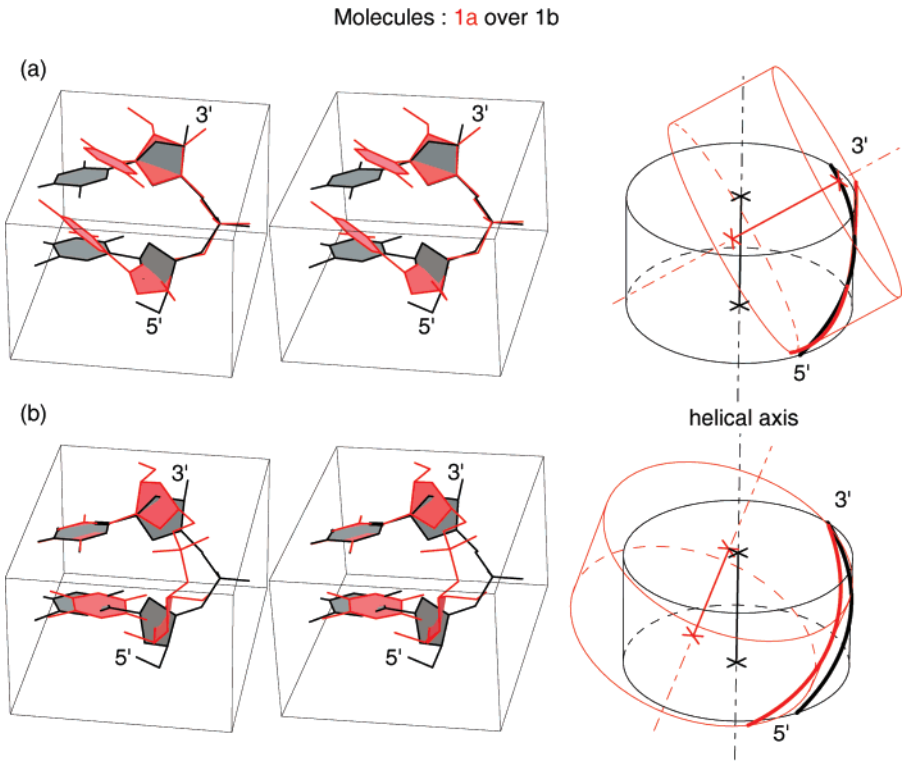

Figure 4. Stereoscopic (left) and schematic (right) views of the average superimposed conformations of **1a** (red lines) and **1b** (black lines) derived from 10 ns MD simulations (shown also in Figures 5 and 6) and represented with the same viewpoint. The molecules were constructed from torsion angles averages of Table 3 and superimposed by adjustment of one of the two sets of atoms: (a) the backbone atoms between the two sugars, 5′(C4′-C3′-O3′)-(P)-3′(O5′-C5′-C4′-C3′); (b) the 3′-base atoms. The schematic views (right) display the A-DNA cylinder (red) around which is wrapped helically the sugar−phosphate chain of **1a** (bold red line) and the B-DNA cylinder (black) around which is wrapped helically that of **1b** (bold black line). Bold helical segments are drawn within the cylinders.

TABLE 4: Average Angles and Torsion Angles in Degrees Describing the Base Stacking Geometry, Computed with Thymine Atoms Involved in the Bond Formation to Yield CPD: $C6_{(1)}-C6_{(2)}$; $C5_{(1)}-C5_{(2)}$ within 1a and 1b from the 10 ns of MD Simulations Used to Compute Tables 2 and 3[a]

	1a 7.7 ns (C3′-*endo*-C3′-*endo*)		**1a** 2.3 ns (C2′-*endo*-C3′-*endo*)		**1b** 10 ns	
θ between the two base planes	16	(8)	27	(15)	15	(12)
$C6_{(1)}C6_{(2)}C2_{(2)}$	104	(12)	108	(17)	89	(17)
$C2_{(1)}C6_{(1)}C6_{(2)}$	69	(13)	66	(15)	78	(13)
$N3_{(1)}C5_{(1)}C5_{(2)}$	80	(16)	70	(19)	91	(15)
$C5_{(1)}C5_{(2)}N3_{(2)}$	92	(15)	103	(22)	75	(18)
$C2_{(1)}C6_{(1)}C6_{(2)}C2_{(2)}$	47	(15)	25	(28)	49	(19)
$N3_{(1)}C5_{(1)}C5_{(2)}N3_{(2)}$	45	(16)	24	(30)	50	(21)
$C6_{(1)}-(C6C5)_{(1)}-(C6C5)_{(2)}-C6_{(2)}$	42	(18)	15	(30)	51	(18)
$C5_{(1)}-(C6C5)_{(1)}-(C4O4)_{(2)}-O4_{(2)}$	39	(23)	7	(32)	45	(20)

[a] Numbers in parentheses correspond to standard deviations from average values; subscript numbers in parentheses correspond to the 5′ residue (1) or to the 3′ residue (2). Notation (C6C5) in the last two lines denotes the midpoint between C6 and C5.

TABLE 5: Average Distances (Angstroms) between the Thymines Atoms Involved in the Formation of CPD ($C6_{(1)}-C6_{(2)}$; $C5_{(1)}-C5_{(2)}$) and (6−4)PP ($C5_{(1)}-O4_{(2)}$; $C6_{(1)}-C4_{(2)}$) Adducts within 1a and 1b from the 10 ns MD Simulations Used to Compute Tables 2−4[a]

interatomic distances	**1a** 7.7 ns C3′-*endo*-C3′-*endo*	**1a** 2.3 ns C3′-*endo*-C2′-*endo*	**1b** 10 ns
$C6_{(1)}-C6_{(2)}$	4.3 (0.5)	4.8 (0.7)	4.3 (0.6)
$C5_{(1)}-C5_{(2)}$	3.9 (0.5)	4.4 (0.7)	4.2 (0.7)
$C5_{(1)}-O4_{(2)}$	4.3 (0.6)	4.5 (0.9)	4.2 (0.8)
$C6_{(1)}-C4_{(2)}$	4.7 (0.5)	4.9 (0.8)	4.3 (0.7)

[a] Numbers in parentheses correspond to standard deviations from average values; subscript numbers in parentheses correspond to the 5′ residue (1) or to the 3′ residue (2).

equidistant from their 3′ base, and (iii) practically located on top of the 3′ base. This shows that the two thymine bases remain well-stacked with a very similar geometry even though the relative positions of the bases and of the backbone are very different in the average conformations of **1a** and **1b**.

These stacking similarities are confirmed quantitatively by MD averages of selected angles (Table 4). Mean and standard deviation values of the angle, θ, between the two base planes are very similar in both molecules. They are close to zero, showing that the base planes are nearly parallel. Angles formed by the line defined by two atoms across one base and the line between two equivalent atoms across the two bases ($C6_{(1)}C6_{(2)}$-$C2_{(2)}$, $C2_{(1)}C6_{(2)}C6_{(2)}$, $N3_{(1)}C5_{(1)}C5_{(2)}$, and $C5_{(1)}C5_{(2)}N3_{(2)}$) are very close in both types of stacking (Table 4). These values show that the two bases are stacked directly onto each other. Torsion angle values of $C6_{(1)}-(C6C5)_{(1)}-(C6C5)_{(2)}-C6_{(2)}$ and of $C5_{(1)}-(C6C5)_{(1)}-(C6C5)_{(2)}-C5_{(2)}$ show that bases stack with the same rotation twist ≈40° in both molecules (Figure 4), a value close to the standard helical twist in B-DNA or A-DNA. Distances between the thymines atoms involved in the formation

of CPD or (6−4)PP are given in Table 5. They are about or slightly longer than the sum of van der Waals radii expected for the stacking of two bases (3.34 Å in DNA or RNA) and are very close for each dinucleotide. Therefore, we must conclude that small variations of backbone torsion angles and of χ compensate for different average values of P and for the different locations of the sugar−phosphate chains in 3-D space to keep the same base stacking geometry. Such a result could be brought about by hydration of the two pyrimidines.

3.4. Dinucleoside Monophosphates 1a and 1b Remain in A or B Form, Respectively. As shown in Figure 5a and as revealed by values of Table 3, the average conformation of dinucleotide **1a** from 10 ns MD possesses the three following

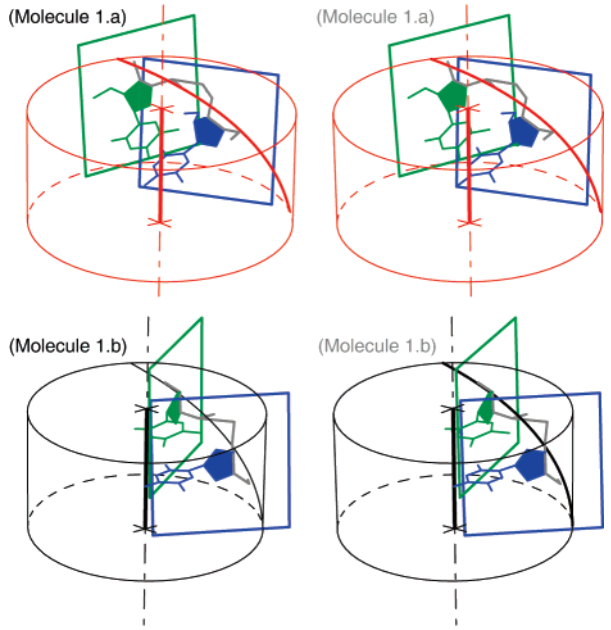

Figure 5. Stereoscopic views of the individual average conformations of **1a** (top) and **1b** (bottom) derived from 10 ns MD simulations. The molecules were constructed from torsion angles averages of Table 3. The sugar−phosphate chains (gray) of **1a** (top) and of **1b** (bottom) are wrapped helically around an A-DNA cylinder (top red) and a B-DNA cylinder (bottom black). 5′-nucleotides are blue and 3′-nucleotides are green. In **1a**, the mean planes of the sugars are tangential to the cylinder of the helix, whereas in **1b** they are contained in radial planes.

main characteristic features of the A-DNA conformation. When the sugar−phosphate chain of this average conformation is fit to a standard A-DNA sugar−phosphate chain of known helix axis and mean radius, we observe first that the mean planes of the sugars are tangential to the cylinder of the helix and second that the base planes are not perpendicular to the helical axis. Third, torsion angle values are also typical of A-DNA conformation. In the same way, the average conformation of dinucleotide **1b** over 10 ns MD possesses the three following main typical features of the B-DNA conformation. When the sugar phosphate chain of this average conformation is fitted to a standard B-DNA of known helix axis and mean radius, we observe first that the sugars and their mean planes point toward the helical axis and second that the base planes are perpendicular to the helix axis (Figure 5b). Third, torsion angle values are also typical of the B-DNA conformation. A closer examination of Figure 5b shows a slightly distorted B-DNA conformation since the mean plane of the 5′-nucleotide is not perfectly radial. These two sets of results show that conformations of **1a** and **1b** belong respectively to the A and B family. However, the similar stacking geometry indicates that double-stranded and single-stranded DNAs are different conformation variations within A and B families for the following reason. In double-stranded DNAs, the stacking of base pairs, considered as an entity, is optimized within the imposed geometry of the double helices.[8b,14c] Therefore, depending on adjacent sequences, the two thymines of two consecutive A.T Watson-Crick base pairs may not stack well on top of each other.[14a] With these dinucleotides, we observe optimal single base stacking. From a structural viewpoint, this suggests that the overall twisting of the single-stranded sugar−phosphate chain required to obtain stacking similarity with two different geometries is easily overcome by interactions that promote stacking: electrostatics, van der Waals, hydrophobicity, or solvent entropy. In brief, the conformations of these single-stranded dinucleotides cannot possess the full features of double-stranded DNAs but retain the main generating principle of optimizing base (not base pair) stacking within the imposed geometry of the A- or B-DNA family in solvent.

3.5. Conformation Results are in Agreement with CD and Photochemical Experiments. It is expected to observe the base planes of stacked bases in an approximately parallel orientation with the known interplay between the torsion angles δ which is directly correlated with P and χ.[11c,d,32] However, it is more surprising to observe that such very similar base stacking geometries (Figure 4b) can be consistent with the different A-DNA and B-DNA conformations (Figure 5). These results are consistent with experimental data for the following reasons: On the one hand, the CD difference spectra between each dimer **1a** and **1b** and its corresponding monomer have the same shape within a constant positive multiplier,[6] as expected if the two-state model applies to **1a** and **1b** and if the geometries of the stacked bases are very similar. Also, an analysis of CD spectra of **1a** and **1b** recorded at different temperatures shows that the fraction of the stacked conformation for **1a** is approximately three times higher than that of **1b** at 20 °C.[6]

On the other hand, they provide an average base stacking geometry that can be discussed in light of the photochemical behavior of **1a** and **1b**.[6] Indeed, excitation of stacked species only gives rise to CPD and (6−4)PP.[6] The CPD photoproduct derives from a (2 + 2) cycloaddition between the two C5−C6 double bonds of thymines whereas the (6−4)PP results from a Paterno−Büchi reaction involving the C5−C6 double bond of the 5′-thymine and the C4 carbonyl of the 3′-thymine. Such a similarity of stacking supports the similar geometry of interaction between the two pyrimidines within **1a** and **1b** and consequently the similar CPD-to-(6−4)PP formation ratio observed between each series in the course of their far UV photolysis.[6] Considering the selectivity of photoproduct formation with respect to the MD-derived base stacking geometry, our results indicate that neither **1a** nor **1b** exhibit a favored distance or geometry leading to the preferential formation of a single type of photoproduct (CPD or (6−4)PP; Table 4). In contrast, some dinucleotide analogues such as peptide nucleic acids (PNAs) possess a conformation such that only CPD are formed upon 254 nm photolysis.[4]

Finally, since the geometries of stacked bases appear to be so similar, one should not only expect the photoproducts to be nearly identical but also expect their rates of formation to be proportional to the concentration of the stacked species. Therefore, the rate of formation of each photoproduct (CPD or (6−4)PP) from **1a** should be about threefold that from **1b**, since the experimental concentration of the stacked species of **1a** is approximately threefold that of **1b**. As given in Table 1, the ratios of the measured quantum yields, **1a** over **1b,** of CPD and of (6−4)PP are respectively 2.7 and 2.15. These values are

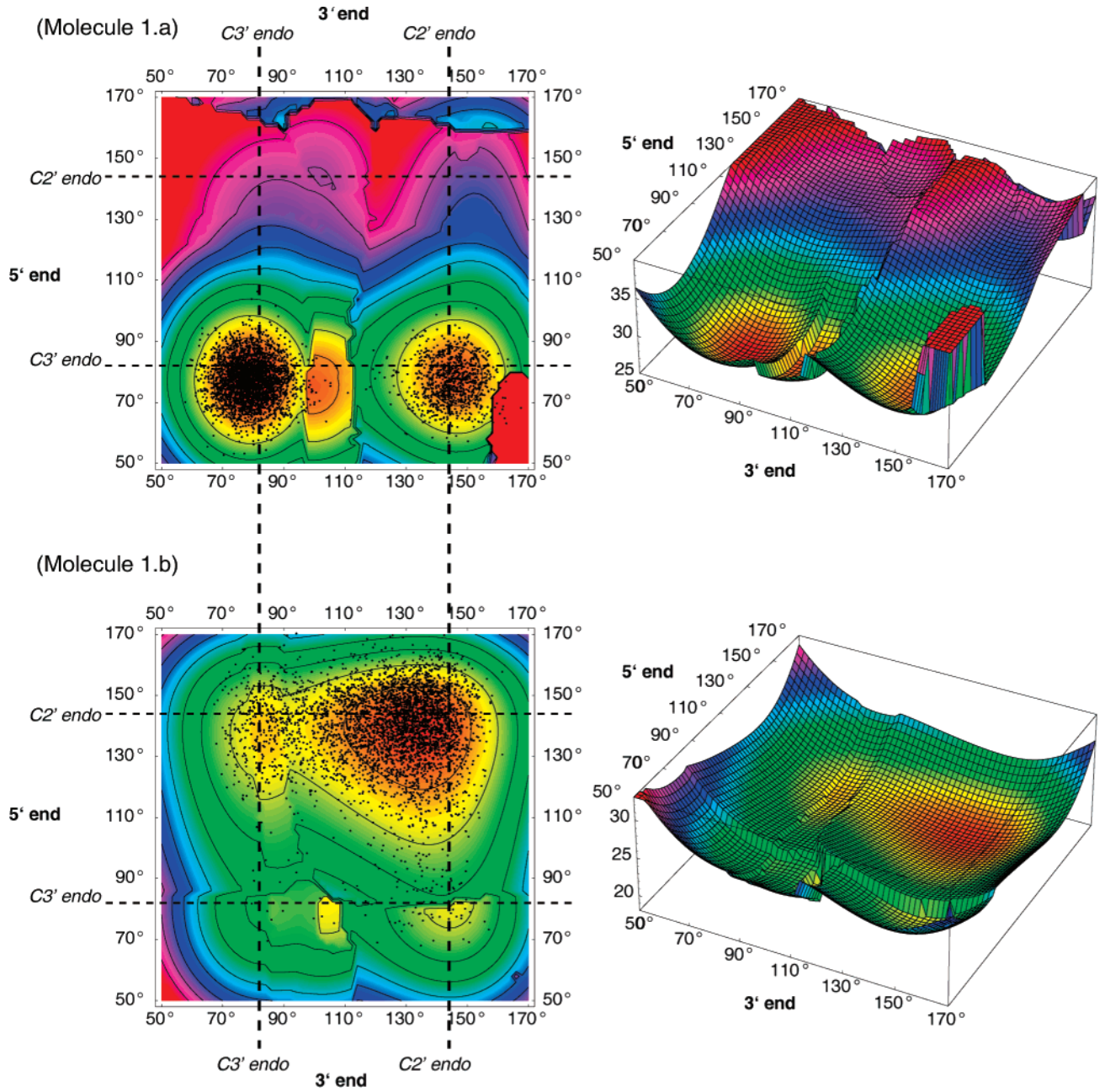

Figure 6. Total energy surfaces of the dinucleoside monophosphates **1a** (top) and **1b** (bottom) in kilocalorie per mole computed as a function of the two torsion angles δ (C5′-C4′-C3′-O3′) and scatter plots of the torsion angles values during 10 ns MD simulations whose average conformations are shown also in Figures 4 and 5. Total energy is represented as two-dimensional contour plots (left) or as three-dimensional surfaces (right). The relationships between the two most common conformations of the sugar ring and angle δ are C3′-*endo*, 82° and C2′-*endo*, 144°. Each energy surface may be conveniently divided into four major areas: C2′-*endo*-C2′-*endo*, C3′-*endo*-C2′-*endo*, C3′-*endo*-C3′-*endo*, and C2′-*endo*-C3′-*endo*.

both sufficiently close to the approximate value of 3 to ensure a good agreement.

3.6. Different Structures and Flexibilities of the A- or B-Form Dinucleoside Monophosphates May Account for Minor Variations in Quantum Yields of Photoproducts Formation. The obtained results are very convincing. However, agreement may not be quantitative. Up to now, our attention was mostly focused on the geometry of stacking. In spite of this remarkable similarity, the whole conformation and the dynamics of the molecules should be taken into account. As shown in Figure 5, dinucleotides **1a** and **1b** adopt respectively the very different geometries of A-DNA and B-DNA. The different average orientations of the sugar rings provide a simple explanation why the bases must fluctuate differently and why they must explore different conformational spaces around a similar stacking conformation. One of simplest methods to explore macromolecular dynamics is to compute the total energy of the molecule by energy minimization as a function of suitable reaction coordinates. This type of calculation is referred to as adiabatic mapping.[28] To estimate the energy costs for transition between A and B conformations, sugar puckers are the required reaction coordinates. The exact conformations of a sugar ring are complex to describe, but they are well-approximated with torsion angle, δ (C5′−C4′−C3′−03′), about the C4′−C3′ bond.[11c,d] As observed in the adiabatic mapping of the pucker conformations of Figure 6a (right), the total potential energy surface of dinucleotide **1a** is the most favorable in the region where both sugars are in C3′-*endo* conformation. As observed with the scatter plot of Figure 6a (left), this is the region where most of the MD of the stacked conformation is confined. The

second best conformation is C3′-*endo*-C2′-*endo*. In Figure 6b, the total potential energy surface of dinucleotide **1b** suggests that the region where both sugars are in the C2′-*endo* conformation is the most favorable, but the region of the conformations where both sugars are not C3′-*endo* can also be sampled during the MD. Comparison of these two behaviors suggests that very different regions of conformational space are explored with different extents. Furthermore, explorations are wider for dinucleotide **1b** than for dinucleotide **1a**.

As shown in Figures 3 and 6, the different structures and structural flexibilities of the stacked conformations of **1a** and **1b** are emphasized by present MD simulations. They could account for the small discrepancy between the ratios of quantum yields for **1a** and **1b**. While **1a** and **1b** have the same average base stacking geometry, the wider conformational dynamics of **1b** could permit a more or less favorable sampling of photoproductive conformational regions.

4. Conclusions

Compound **1a** was initially synthesized to induce a strong conformational bias toward C3′-*endo* conformation and therefore to force the stacked molecule into an A conformation. Unexpectedly, **1a** and **1b** gave rise to the same photoproducts with however a two- to threefold higher yield. Our investigations of the molecular conformations of **1a** and **1b** by MD in aqueous solvent and by adiabatic mapping suggest the following conclusions to account for this observation and for the detailed experimental results obtained before.[6] (1) Stacked dinucleotides **1a** and **1b** adopt the main characteristic features of single-stranded A and B forms, respectively, as initially sought and in agreement with NMR measurements. (2) Unexpectedly, stacking geometries of thymines in dinucleotides **1a** and **1b** are very similar in MD simulation with explicit aqueous solvent. This result explains nicely at the same time, the similarity of CD difference spectra and the similarity of the photoproducts of **1a** and **1b**. It is also in line with the finding that the ratio of the quantum yields of formation of CPD and (6−4)PP from **1a** over **1b** (2.7 and 2.15, respectively) is close to 3, the estimated ratio of the corresponding stacked species. (3) However, the measured quantum yield ratios could be marginally different because of the different structures and flexibilities of the stacked conformations of **1a** and **1b** and different explorations of conformational space as recorded by MD and adiabatic mapping for **1a** and **1b**. (4) Many studies have been conducted on dinucleotides and on thymine dinucleotides, and yet their conformations have not been established in detail. Thanks to state-of-the-art nanosecond MD simulations in explicit solvent, it is now possible not only to gain a thorough explanation for the above-described conformation paradox but also to retrieve average conformations that account for most of known conformational behaviors. Stacking geometry and photochemistry in double helical DNA are complex and depend on neighboring bases.[33] In contrast, stacked dinucleotide TpT may now offer a simple model with well-characterized geometry. Therefore, the average stacked conformations that we observed on 10 ns time scales could serve as good starting models to investigate photochemical reactions with quantum dynamics simulations. Other thymine dinucleotide analogues are under study to characterize different average conformations related to different photoproduct formation. It is expected that these studies combined with adiabatic maps and MD simulations will be helpful to predict and understand the selectivity of photochemical reactions between nucleobases.

Acknowledgment. We thank the University P. & M. Curie and the CNRS (PCV 2000) for financial support. G.P.H.S. acknowledges support from the Association pour la Recherche sur le Cancer (ARC) and from the University P. & M. Curie Paris 6 (ATER).

References and Notes

(1) (a) http:/www.cancer.org, 2007. (b) Patrick, M. H.; Rahn, R. O. In *Photochemistry and Photobiology of Nucleic Acids: Photochemistry of DNA and Polynucleotides: Photoproducts*; Wang, S. Y., Ed.; Academic Press: New York, 1976; Vol. 2, pp 35−95. (c) Pfeifer, G. P. *Photochem. Photobiol.* **1997**, *65*, 270−283.

(2) (a) Cleaver, J. E.; Crowley, E. *Front. Biosci.* **2002**, *7*, d1024−1043. (b) Zhao, X.; Taylor, J.S.; *Nucleic Acids Res.* **1996**, *24*, 1561−1565.

(3) (a) Mohr, S. C.; Sokolov, N. V. H. A.; He, C.; Setlow, P. *Proc. Natl. Acad. Sci. U.S.A.* **1991**, *88*, 77−81. (b) Nicholson, W. L.; Setlow, B.; Setlow, P. *Proc. Natl. Acad. Sci. U.S.A.* **1991**, *88*, 8288−8292. (c) Douki, T.; Court, M.; Sauvaigo, S.; Odin, F.; Cadet, J. *J. Biol. Chem.* **2000**, *275*, 11678−11685. (d) Becker, M.; Wang, Z. *J. Mol. Biol.* **1989**, *210*, 429−438. (e) Cadet, J.; Vigny, P. In *Bioorganic Photochemistry*; Morrison, H., Ed.; Wiley & Sons: New York, 1990; pp 1−272.

(4) Clivio, P.; Guillaume, D. *Tetrahedron Lett.* **1998**, *39*, 6881−6884.

(5) Thomas, M.; Clivio, P.; Guillaume, D.; Fourrey, J.-L. *Nucleosides, Nucleotides Nucleic Acids* **2001**, *20*, 927−929.

(6) Ostrowski, T.; Maurizot, J.-C.; Adeline, M.-T.; Fourrey, J.-L.; Clivio, P. *J. Org. Chem.*, **2003**, *68*, 6502−6510.

(7) (a) Bensasson, R. V.; Land, E. J.; Truscott, T. G. In *Excited states and free radicals in biology and medecine: contributions from flash photolysis and pulse radiolysis*; Oxford University Press: Oxford, U.K., 1993; pp 154−155. (b) Ruzsicska, B. P.; Lemaire, D. G. E. In *UCRC Handbook of Organic Photochemistry and Photobiology*; Horspool, W. M., Song, P.-S., Eds.; Elsevier CRC Press: Boca Raton, FL, 1995; pp 1289−1317.

(8) (a) Bloomfield, V. A.; Crothers, D. M.; Tinoco, I., Jr. *Physical Chemistry of Nucleic Acids, Structures*; Harper & Row: New York, 1974; pp 66−101. (b) Bloomfield, V. A.; Crothers, D. M.; Tinoco, I., Jr. *Nucleic Acids, Structures, Properties, and Functions;* University Science Books: Sausalito, CA, 2000; pp 13−43. (c) Cantor, C. R.; Schimmel, P. R. *Biophysical Chemistry Part I: The conformation of biological macromolecules;* Freeman: San Francisco, CA, 1980; pp 311−341. (d) Cantor, C. R.; Schimmel, P. R. *Biophysical Chemistry Part III: The behavior of biological macromolecules;* Freeman: San Francisco, CA, 1980; pp 1211−1214.

(9) Ts'o, P. O. P., Ed. *Basic Principles in Nucleic Acid Chemistry;* Springer-Verlag: New York, 1974; pp 453−584.

(10) (a) Hartel, A. J.; Lankhorst, P. P.; Altona, C. *Eur. J. Biochem.* **1982**, *129*, 343−357.

(11) (a) Saenger, W. In *Principles of Nucleic Acid Structure;* Cantor, C. R., Ed.; Springer-Verlag: New York, 1984; pp 134−137; (b) Chapter 9−11; (c) Chapters 2 and 4. (d) Dickerson, R. E; Kopka, M. L.; Pjura, P. In *Biological Macromolecules and Assemblies*; Jurnak, F. A., McPherson, A., Eds.; John Wiley & Sons: New York, 1885; Vol. 2, pp 38−126.

(12) Lesnik, E. A.; Freier, S. M. *Biochemistry* **1998**, *37*, 6991−6997.

(13) (a) Lee, C.-H.; Ezra, F. S.; Kondo, N. S.; Sarma, R. H.; Danyluk, S. S. *Biochemistry* **1976**, *15*, 3627−3638. (b) Cheng, D. M.; Sarma, R. H. *J. Am. Chem. Soc.* **1977**, *99*, 7333−7348. (c) Cheng, D. M.; Sarma, R. H. *Biopolymers* **1977**, *16*, 1687−1711. (d) Kawai, G.; Yamamoto, Y.; Kamimura, T.; Masegi, T.; Sekine, M.; Hata, T.; Iimori, T.; Watanabe, T.; Miyazawa, T.; Yokoyama, S. *Biochemistry* **1992**, *31*, 1040−1046.

(14) (a) Jurnak, F.; McPherson, A., Eds. *Biological Macromolecules and Assemblies, Vol. 2: Nucleic Acids and Interactive Proteins*; John Wiley and Sons: New York, 1985. (b) Neidle, S., Ed. *Oxford Handbook of Nucleic Acid Structure*; Oxford University Press: New York, 1999; Chapters 1, 2, 5, and 6. (c) Calladine, C. R.; Drew, H. R.; Luisi, B. F.; Travers, A. A. *Understanding DNA;* Elsevier Academic Press: Amsterdam, The Netherlands, 2004; pp 39−63. (d) Olson, W. K.; Bansal, M.; Burley, S. K.; Dickerson, R. E.; Gerstein, M.; Harvey, S. C.; Heinemann, U.; Lu, X.-J.; Neidle, S.; Shakked, Z.; Sklenar, H.; Suzuki, M.; Tung, C.-S.; Westhof, E.; Wolberger, C.; Berman, H. M. *J. Mol. Biol.* **2001**, *313*, 229−237.

(15) Kool, E. T. *Annu. Rev. Biophys. Biomol. Struct.* **2001**, *30*, 1−22.

(16) (a) Yathindra, N.; Sundaralingam, M. *Biopolymers* **1975**, *14*, 2387−2399. (b) Broyde, S.; Stellman, S. D.; Hingerty, B. *Biopolymers* **1978**, *17*, 1485−1506. (c) Thiyagarajan, P.; Ponnuswamy, P. K. *Biopolymers* **1978**, *17*, 533−553.

(17) (a) Norberg, J.; Nilsson, L. *Biophys. J.* **1998**, *74*, 394−402. (b) Norberg, J.; Nilsson, L. *J. Am. Chem. Soc.* **1995**, *117*, 10832−10840. (c) Norberg, J.; Nilsson, L. *Biophys. J.* **1994**, *67*, 812−824.

(18) (a) Miller, J. L.; Cheatham, T. E., III; Kollman, P. A. In *Oxford Handbook of Nucleic Acid Structure;* Neidle, S., Ed.; Oxford University Press: New York, 1999; pp 95−116. (b) Wang, W.; Donini, O.; Reyes, C. M.; Kollman, P. A. *Annu. Rev. Biophys. Biomol. Struct.* **2001**, *30*, 211−

243. (c) Kollman, P. A.; Massova, I.; Reyes, C.; Kuhn, B.; Huo, S.; Chong, L.; Lee, M.; Lee, T.; Dyan, Y.; Wang, W.; Donini, O.; Cieplak, P.; Srinivasan, J.; Case, D. A.: Cheatham, T. E., III *Acc. Chem. Res.* **2000**, *33*, 889−897.

(19) Luo, R.; Gilson, H. S. R.; Potter, M. J.; Gilson, M. K. *Biophys. J.* **2001**, *80*, 140−148.

(20) (a) Norberg, J.; Nilsson, L. *J. Chem. Phys.* **1996**, *4*, 6052−6057. (b) Auffinger, P.; Westhof, E. *J. Mol. Biol.* **2000**, *300*, 1113−1131. (c) Auffinger, P.; Westhof, E. *J. Mol. Biol.* **2001**, *305*, 1057−1072. (d) Pan, Y.; Mackerell, A. D., Jr. *Nucleic Acids Res.* **2003**, *31*, 7131−7140. (e) Noy, A.; Pérez, A.; Lankas, F.; Luque, F. J.; Orozco, M. *J. Mol. Biol.* **2004**, *343*, 627−638.

(21) Auffinger, P.; Vaiana, A. C. In *Handbook of RNA Biochemistry Molecular dynamics of RNA systems*; Hartmann, R. K., Bindereif, A., Schön, A., Westhof, E., Eds.; Wiley-VCH: Weinheim, Germany, 2005; pp 560−576.

(22) (a) Johns, H. E.; Pearson, M. L.; LeBlanc, J. C.; Helleiner, C. W. *J. Mol. Biol*., **1964**, *9*, 503−524. (b) Cantor, C. R.; Schimmel, P. R. *Biophysical Chemistry Part II: Techniques for the study of biological structure and function*; Freeman: San Francisco, CA, 1980; Chapter 7, pp 349−408. (c) Bloomfield, V. A.; Crothers, D. M.; Tinoco, I., Jr. *Physical Chemistry of Nucleic Acids, Structures*; Harper & Row: New York, 1974; p 133. (d) Cantor, C. R.; Warshaw, M. M.; Shapiro, H. *Biopolymers* **1970**, *9*, 1059−1077.

(23) (a) Case, D. A.; Pearlman, D. A.; Caldwell, J. W.; Chearham, T. E.; Ross, W. S.; Simmerling, C. L.; Darden, T. A.; Merz K. M.; Stanton, R. V. Cheng, A. L.; Vincent, J. J.; Crowley, M.; Fergusson, D. M.; Radmer, R. J.; Seibel, G. L.; Singh, U. C.; Weiner, P. K.; Kollman, P. A. University of California: San Francisco, CA, 1997. (b) Cheatham, T. E., III; Cieplak, P.; Kollman, P. A. *J. Biomol. Struct. Dyn.* **1999**, *16*, 845−861.

(24) Venkateswarlu, D.; Lind, K. E.; Mohan, V.; Manoharan, M.; Ferguson, D. M. *Nucleic Acids Res.* **1999**, *27*, 2189−2195.

(25) Arnott, S.; Smith, P. J. C.; Chandrasekaran, R. In *Atomic Coordinates and Molecular Conformations for DNA−DNA, RNA−DNA, and DNA−RNA Helices*, Vol. 2; Fasman, G. D., Ed.; CRC Press: Cleveland, OH, 1976; pp 411−422.

(26) Cognet, J. A. H.; Boulard, Y.; Fazakerley, G. V. *J. Mol. Biol.* **1995**, *246*, 209−226.

(27) Santini, G. P. H; Pakleza, C.; Cognet, J. A. H. *Nucleic Acids Res.* **2003**, *31*, 1086−1096.

(28) McCammon, J. A.; Harvey, S. A. *Dynamics of Proteins and Nucleic Acids*; Cambridge University Press: Cambridge, U.K., 1987.

(29) Cognet, J. A. H.; Gabarro-Arpa, J.; Cuniasse, P.; Fazakerley, G. V.; Le Bret, M. *J. Biomol. Struct. Dynam.* **1990**, *7*, 1095−1115.

(30) (a) Yathindra, N.; Sundaralingam, M. *Biopolymers* **1979**, *18*, 2721−2731. (b) Prusiner, P.; Yathindra, N.; Sundaralingam, M. *Biochim. Biophys. Acta* **1974**, *18*, 115−123.

(31) Norberg, J.; Nilsson, L. *Biophys. J.* **1995**, 69, 2277−2285.

(32) Pearlman, D. A.; Kim, S.-H. *J. Biomol. Struct. Dyn.* **1986**, *4*, 49−67.

(33) (a) Crespo-Hernandez, C.; Cohen, B.; Kohler, B. *Nature* **2005**, *436*, 1141−1144. (b) Markovitsi, D.; Talbot, F.; Gustavsson, T.; Onidas, D.; Lazzarotto, E.; Marguet, S., *Nature* **2006**, *441*, E7, DOI:10.1038/nature04903.